



## OPEN ACCESS

## EDITED BY

Federico Ricci-Tersenghi,  
Sapienza University of Rome, Italy

## REVIEWED BY

Qiang Zhai,  
Xi'an Jiaotong University, China  
Luca Leuzzi,  
National Research Council (CNR), Italy

## \*CORRESPONDENCE

R. L. Orbach,  
✉ orbach@utexas.edu

RECEIVED 14 January 2024

ACCEPTED 20 February 2024

PUBLISHED 20 March 2024

## CITATION

He J and Orbach RL (2024), Spin glass dynamics  
through the lens of the coherence length.  
*Front. Phys.* 12:1370278.  
doi: 10.3389/fphy.2024.1370278

## COPYRIGHT

© 2024 He and Orbach. This is an open-access  
article distributed under the terms of the  
[Creative Commons Attribution License \(CC BY\)](https://creativecommons.org/licenses/by/4.0/).  
The use, distribution or reproduction in other  
forums is permitted, provided the original  
author(s) and the copyright owner(s) are  
credited and that the original publication in this  
journal is cited, in accordance with accepted  
academic practice. No use, distribution or  
reproduction is permitted which does not  
comply with these terms.

# Spin glass dynamics through the lens of the coherence length

J. He and R. L. Orbach\*

Texas Materials Institute, The University of Texas at Austin, Austin, TX, United States

Spin glass coherence lengths can be extracted from experiment and from numerical simulations. They encompass the correlated region, and their growth in time makes them a useful tool for exploration of spin glass dynamics. Because they play the role of a fundamental length scale, they control the transition from the reversible to the chaotic state. This review explores their use for spin glass properties, ranging from scaling laws to rejuvenation and memory.

## KEYWORDS

spin glass dynamics, coherence length, rejuvenation, memory, numerical simulation, scaling law

## 1 Introduction

The dynamical processes found in spin glasses mimic those from a wide variety of physical systems, not limited to glass formers, polymers, granular materials, phase separation in the early Universe, and the social sciences. Because their dynamical properties can be measured directly, they provide a window into the behavior of far-from-equilibrium systems. This review will explore the spin glass coherence length,  $\xi(t, t_w; H)$ , its definition, extraction from experiment and simulations, and applications. Here,  $t_w$  is the age of the spin glass system before the measurement time,  $t$  begins, and  $H$  is the magnetic field. An inherent advantage of the use of  $\xi(t, t_w; H)$  to describe dynamical properties is that the spin glass transition temperature,  $T_g$  is implicit. A precise value of  $T_g$  is not required even for explorations close to  $T_g$ .

The first explicit experimental procedure for extraction of the spin glass was proposed and demonstrated by Joh et al. [1]. They noted that the relevant free energy barrier energy change from imposition of a magnetic field  $H$  was given by what they termed the “Zeeman” energy,  $E_Z$  where,

$$E_Z = N_s \chi_{FC} H^2 . \quad (1)$$

Here,  $N_s$  is the number of spins in a volume subtended by  $\xi(t, t_w; H)$ , and  $\chi_{FC}$  is the field-cooled susceptibility *per spin*. They took  $N_s = (4/3)\pi[\xi(t, t_w; H)]^3$  whereas, subsequently, a value based on the structure of the four spin coherence length was introduced [2],

$$N_s = [\xi(t, t_w; H)]^{D-(\theta/2)} \quad (2)$$

where  $\theta$  is the replicon exponent [3].

The Sherrington-Kirpatrick (SK) infinite range exchange Hamiltonian [4] for spin glasses exhibits states within an ultrametric geometry [5] which has a pictorial equivalent [6] of an hierarchical organization. Free energy barriers separate states with occupancies that increase exponentially with diminishing overlap. The Parisi solution [7, 8] of the SK model are “pure states” separated by infinite barriers. This geometry was shown by analogy to replicate dynamical transitions between states with finite free energy barriers [9]. Putting

all these factors together leads to an inflection point in the time dependence of the magnetization, and hence a maximum in the logarithmic derivative of the time dependent magnetization, known as  $S(t, t_w; H)$ , the relaxation function:

$$S(t, t_w; H) = \frac{dM(t, t_w; H)}{d \ln t} \quad (3)$$

Experimentally, the magnetization is measured at constant temperature  $T$  after an aging time  $t_w$ . Empirically, the maximum of  $S(t, t_w; H)$  occurs at a time  $t \approx t_w$  [10] associated with the largest free energy barrier generated by the growth of the spin glass coherence length  $\xi(t, t_w; H)$  where  $H$  is the magnetic field.

In a thermoremanent magnetization (TRM) experiment,  $H$  is applied in the paramagnetic state, kept constant as the spin glass is cooled to a temperature  $T$  below the condensation temperature  $T_g$ , and the magnetization is measured after the time  $t_w$  when  $H$  is changed (most often, cut to zero). In a zero-field cooled (ZFC) experiment,  $H = 0$  initially as the spin glass is cooled to  $T$ , and the magnetization measured upon application of  $H$  after the time  $t_w$ . It is important to understand that the free energy barriers are not “chemical” in their origin. Rather, they are created by larger and larger numbers of correlated spins, the volume containing  $N_s$  subtended by  $\xi(t, t_w; H)$  according to Eq. 2.

Thus, the maximum free energy barrier height,  $\Delta_{\max}$  is associated with  $t_w$  according to an Arrhenius law,

$$\Delta_{\max} \approx k_B T \ln \left[ \frac{t_w}{\tau_0} \right] \quad (4)$$

where  $\tau_0$  is an exchange time usually taken as  $\hbar/k_B T_g$ . From Eq. 1, we can define an “effective” waiting time  $t_w^{\text{eff}}$  in the presence of a magnetic field as,

$$\Delta_{\max} - N_s \chi_{\text{FC}} H^2 = k_B T \ln t_w^{\text{eff}} - k_B T \ln \tau_0, \quad (5)$$

where  $t_w^{\text{eff}}$  is taken as the time when  $S(t, t_w; H)$  reaches its peak in the absence/presence of  $H$  for TRM/ZFC experiments, respectively.

Combining Eqs 1, 5 enables the only means for extraction of the spin glass coherence length from experiment. In order to keep this value explicit, we shall label it  $\xi_{\text{Zeeman}}$ .

Mathematical simulations from the Janus Collaboration [11], using a special purpose computer, can address the value of  $\xi$  directly. In temperature cycling experiments that will be addressed below, they project (at least) two different coherence lengths [12].

The first is  $\xi_{\text{micro}}(t_w, T)$ , the microscopic coherence length computed directly from the replicon propagator [13, 14] in Eq. 6

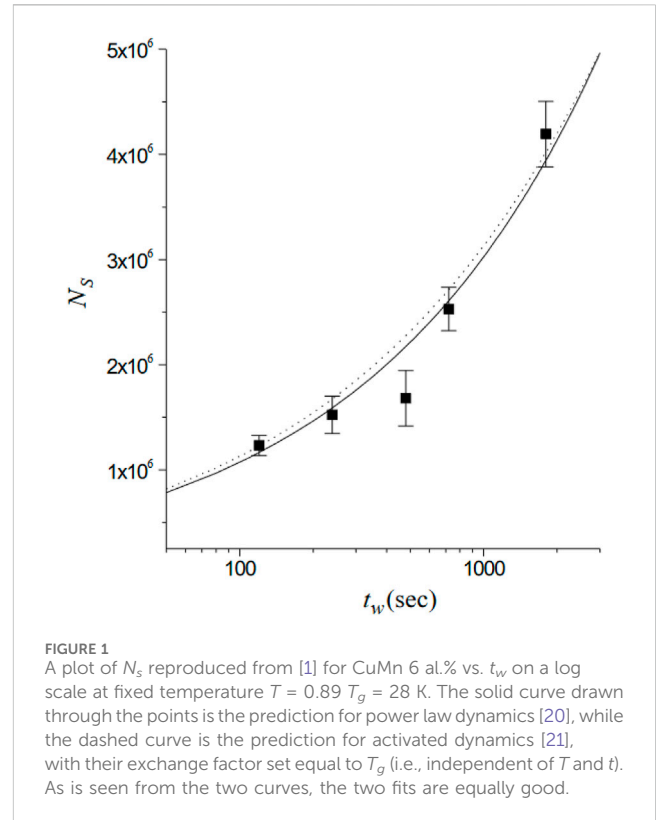
$$\mathcal{G}_R(\mathbf{r}, t, T) = \frac{1}{V} \sum_{\mathbf{x}} \overline{\langle \langle s_{\mathbf{x},t} s_{\mathbf{x}+\mathbf{r},t} \rangle_T - \langle s_{\mathbf{x},t} \rangle_T \langle s_{\mathbf{x}+\mathbf{r},t} \rangle_T \rangle^2}, \quad (6)$$

where for Ising spins,  $s_x = \pm 1$ . The replicon correlator  $\mathcal{G}_R$  decays to zero in the long-distance limit. One therefore computes  $\xi_{\text{micro}}(t_w, H)$  by exploiting the integral estimators [15, 16] in Eqs 7 and 8

$$I_k(t, T) = \int_0^\infty dr r^k \mathcal{G}(\mathbf{r}, t; T), \quad (7)$$

and

$$\xi_{k,k+1}(t, T) = \frac{I_{k+1}(t, T)}{I_k(t, T)}. \quad (8)$$



The  $\xi_{1,2}(t_w, T)$  is designated as the microscopic coherence length  $\xi_{\text{micro}}(t_w, T)$ .

Physically [12], “ $\xi_{\text{micro}}(t_w, T)$  is the size of the (glassy) domains within the sample (it is the largest length scale at which we can regard the system as ordered at time  $t_w$ .”

Another length scale is introduced in simulations [12] when comparing the same system at two times  $t_1$  and  $t_2$  ( $t_1 < t_2$ ):  $\zeta(t_1, t_2)$ . It “characterizes the long-distance decay of the pair-correlation function corresponding to the set of spins taking opposite signs at times  $t_1$  and  $t_2$ . Physically,  $\zeta(t_1, t_2)$  is the typical size of regions where coherent rearrangements have occurred between times  $t_1$  and  $t_2$  . . . because of the ongoing formation of a new spin order at time  $t_2$ . For fixed  $t_1$ ,  $\zeta(t_1, t_2)$  grows with  $t_2$  starting from  $\zeta(t_1, t_2 = t_1) = 0$ .”

At a given temperature,  $\xi_{\text{Zeeman}}(t_w, T)$  “fairly closely follows the behavior of the microscopic length  $\xi_{\text{micro}}(t_w, T)$ ” [12, 17–19] so that, for all practical purposes, they can be taken equal. For varying temperature protocols, the scenario is more intricate because of the presence of temperature chaos at large temperature changes. The length scales are quantitatively compared in Figure 5 of [18].

Now that we have defined the relevant length scales, we show in the next section how they elucidate the dynamical properties of spin glasses.

## 2 Physical properties

The first experimental extraction of  $\xi_{\text{Zeeman}}(t_w, T)$  [1] compared results from two approaches: power law dynamics

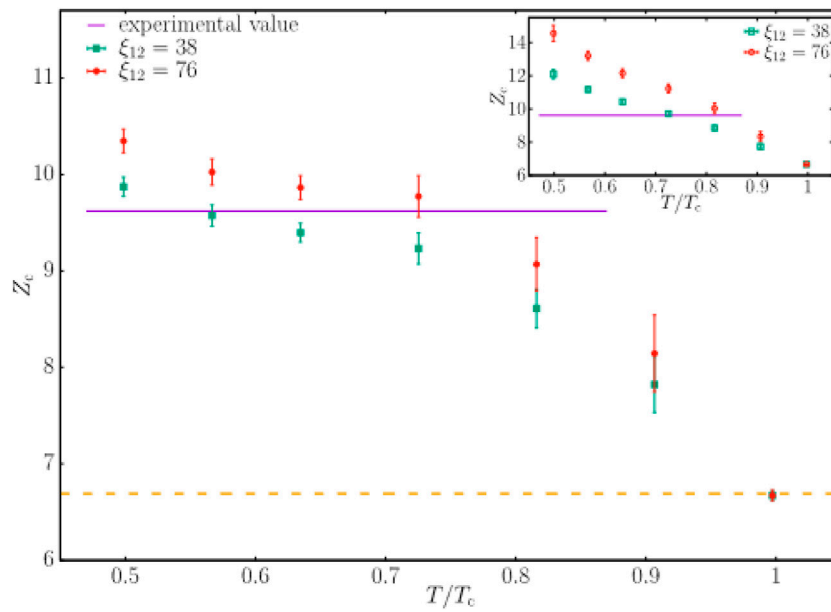


**FIGURE 2** Value of the experimental aging rate for spin glasses  $z_c(T) = z_c(T, \xi)T/T_g$ , reproduced from Ref. [22]. The straight line is the experimental value of  $z_c(T) \approx 9.62$  from Ref. [23].

[20] vs. activated dynamics [21]. The results are reproduced in Figure 1. Knowing  $\chi_{FC}$  per spin from other measurements allows for the extraction of  $\xi_{Zeeman}(t_w, T)$  from Eq. 2. For example, from Figure 1 at  $t_w = 1,000$  s,  $N_s \approx 3 \times 10^6$  spins. They set  $\xi(t_w, T) \approx [N_s(t_w, T)]^{1/3}$  giving  $\xi(t_w = 1,000, T = 28 \text{ K}) = 100 a_0$ , where  $a_0$  is the average distance between Mn ions. Subsequently it was shown [3] that the correct extraction of  $\xi(t_w, T)$  is given by  $[N_s(t_w, T)]^{1/d_f}$ , where  $d_f$  is the fractal dimension equal to  $D - (\theta/2)$ , with  $\theta$  the replicon exponent [16]. In general,  $\theta \sim 0.3-0.4$  so that its omission in Ref. [1] results in only a small error.

The uses of  $\xi(t_w, T)$  to describe physical processes provides a powerful quantitative tool. Pertinent examples are described below.

### 2.1 Slowing down of the growth of $\xi(t_w, T)$

The Janus Collaboration utilizes a special purpose-built computer [16] to examine the dynamics of the Ising spin glass. They were able to explore the (re-normalized) aging rate [22],

$$z_c(T, \xi) = \frac{T}{T_g} \frac{d \ln t_w}{d \ln \xi} \tag{9}$$

The re-normalizing factor  $T/T_g$  makes  $z_c(T, \xi) \approx z_c(\xi)$  [23].

We can rewrite Eq. 9 as Eq. 10,

$$\ln t_w = \frac{z_c T_g}{T} \ln \xi + \text{const} \tag{10}$$

The aging rate,  $z_c$ , was found to vary substantially from experiment to experiments, depending upon the temperature and nature of the spin glass sample. For example, for a bulk polycrystalline sample of CuMn (6 at%) [1] found  $z_c = 5.917$  at a reduced temperature of  $T/T_g$

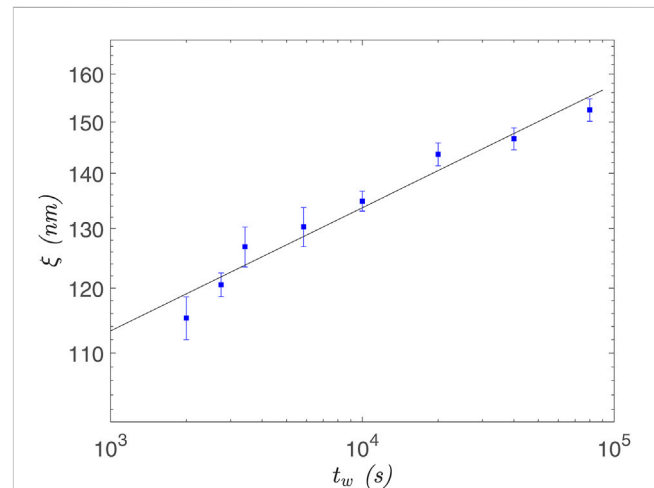


**FIGURE 3**  $\xi(t_w, T)$  as a function of the waiting time  $t_w$  at a measuring temperature of  $T = 28 \text{ K}$  ( $T_g = 31.5 \text{ K}$ ) reproduced from Ref. [26]. The straight line is a fit to  $\ln t_w = (z_c T_g / T) \ln \xi + \text{const}$ . [recall Eq. 10], yielding  $z_c = 12.37 \pm 1.07$ .

$T_g = 0.89$ . For a polycrystalline bulk spinel they found  $z_c = 7.576$  at a reduced temperature of  $T/T_g = 0.72$ .

In thin films [24] found for 11.7 at. % that  $z_c = 9.62$  at reduced temperatures of  $T/T_g = 0.43, 0.59$ , and  $0.78$ . Working at  $T/T_g = 0.95$  [25], found  $z_c = 6.80$  in bulk polycrystalline CuMn (5 at%).

The Janus collaboration [22] found a hint to reconcile these apparently conflicting values from experiment by computing  $\xi$  over a temperature range  $0.5 \leq T/T_g \leq 1$ . Figure 2 exhibits their results.

Experimentally, there is a significant confirmation for this variation of  $z_c$ . Ref. [22] found that the growth of  $\xi(t_w, T)$  slows down as  $\xi(t_w, T)$  increases. That is,  $z_c$  increases as  $\xi(t_w, T)$  increases.

In order to achieve large values of  $\xi(t_w, T)$  to test this simulation prediction, we were blessed with a single crystal of CuMn, 6 at%, grown by Dr. D.L.Schagel, the description of which is contained in Ref. [26]. By working at 28 K ( $T_g = 31.5$  K) and at long waiting times (up to 10<sub>5</sub> s), the value extracted for  $\xi(t_w, T)$  reached 150 nm, the largest coherence length ever reported for a glassy system [26]. The value of  $\xi(t_w, T)$  vs.  $t_w$  is plotted in Figure 3, from which  $z_c = 12.37 \pm 1.07$  can be extracted. This is to be compared with  $z_c \approx 9.62$  extracted at shorter waiting times for smaller values of  $\xi(t_w, T)$ .

## 2.2 Scaling law

The coherence length  $\xi(t_w, T)$  can be measured precisely for spin glasses both in experiment and through simulations. However, known analysis methods lead to discrepancies either for large external magnetic fields or close to the transition temperature. This problem can be solved through introduction of a scaling law that takes into account both the magnetic field and the time-dependent coherence length. This is especially important because temperatures  $T \approx T_g$  are most relevant for the study of glass formers ( $\xi$  is restricted to a very narrow window of variation if one moves away from  $T_g$ ).

Historically, non-linear magnetization effects, and their scaling properties in spin glasses, were first introduced by Malozemoff, Barbara, and Imry [27–29] who introduced the relation for the singular part of the magnetic susceptibility,

$$\chi_s = H^{2/\delta} f(t_r/H^{2/\phi}), \quad (11)$$

where  $f(x)$  is a constant for  $x \rightarrow 0$ ;  $f(x) = x^{-\gamma}$  for  $x \rightarrow \infty$ ;  $\phi = \gamma\delta/(\delta - 1) \equiv \beta\delta$ ; and  $t_r$  is the reduced temperature  $T/T_g$ .

This form was used by Lévy and Ogielski [30], and Lévy [31] who measured the AC non-linear susceptibilities of very dilute AgMn alloys above and below  $T_g$  as a function of frequency, temperature, and magnetic field. Their critical exponents from Eq. 11 differed substantially from Monte Carlo simulations for short-range Ising systems [32]. The discrepancy in their value of  $\gamma$  was very large, and most probably arose from the lack of an exact value for  $T_g$  in their experiments. This illustrates the value of and need for a different approach for scaling the non-linear magnetization of spin glasses in the vicinity of  $T_g$ .

The scaling argument goes as follows. Let  $M(t, t_w; H)$  be the magnetization per spin. The generalized susceptibilities  $\chi_1, \chi_3, \chi_5, \dots$  are defined through the Taylor expansion,

$$M(H) = \chi_1 H + \frac{\chi_3}{3!} H^3 + \frac{\chi_5}{5!} H^5 + \mathcal{O}(H^7). \quad (12)$$

We have omitted  $t$  and  $t_w$  for brevity. Our hypothesis is that, in the non-equilibrium regime for a spin glass close to  $T_g$  in the presence of a small magnetic field,

$$M(t, t_w; H) = [\xi(t + t_w)]^{\gamma_H - D} \times \mathcal{F}\left(H[\xi(t + t_w)]^{\gamma_H}, \frac{\xi(t + t_w)}{\xi(t_w)}\right) \quad (13)$$

According to full-aging spin-glass dynamics [30] Eq. 13 tells us that  $\xi(t + t_w)/\xi(t_w)$  will be approximately constant close to the maximum of the relaxation rate [i.e., peak of  $S(t)$ ], so that we omit this dependence. Thus, combining Eqs 12, 13, one can express the

generalized susceptibilities  $\chi_1, \chi_3, \chi_5, \dots$  in terms of the spin glass coherence length  $\xi(t, t_w; H)$ :

$$\chi_{2n-1} \propto |\xi(t_w)|^{2n\gamma_H - D}, \quad (14)$$

where we have omitted the arguments  $t$  and  $H$  for convenience, and Eq. 15

$$2\gamma_H = D - \frac{\theta(\bar{x})}{2}, \quad (15)$$

with  $\theta(\bar{x})$  the replicon exponent [3].

The first term of  $M(H)$  in Eq. 12 is  $\chi_1$ , which contains the linear term as well as the first non-linear scaling term, so that we write,

$$\chi_1 = \frac{\hat{S}}{T} + \frac{a_1(T)}{\xi^{\theta(\bar{x})/2}} \quad (16)$$

where  $a_1(T)$  is some unknown constant, hopefully varying smoothly with temperature.

The free-energy variation per spin in the presence of a magnetic field can be derived by integrating the magnetic density Eq. 12 with respect to the magnetic field in Eq. 17,

$$\Delta F = -\left[\frac{\chi_1}{2} H^2 + \frac{\chi_3}{4!} H^4 + \frac{\chi_5}{6!} H^6 + \mathcal{O}(H^8)\right]. \quad (17)$$

Substituting the scaling from Eqs 14, 16, the free energy  $\Delta F$  can be written as (we drop the  $\bar{x}$  dependence of  $\theta$  for brevity) in Eq. 18,

$$\Delta F = -\left[\frac{\hat{S}}{2T} H^2 + \frac{a_1(T)}{\xi^{\theta/2}} H^2 + a_3(T) \xi^{D-\theta} H^4 + a_5(T) \xi^{2D-(3\theta/2)} H^6 + \mathcal{O}(H^8)\right], \quad (18)$$

where again the  $a_n(T)$  are unknowns and hopefully again smoothly varying functions of temperature. Using the effective response time,  $t_H^{\text{eff}}$ , to reflect the total free-energy change at magnetic field  $H$  with respect to  $H \rightarrow 0^+$ ,

$$\ln\left[\frac{t_H^{\text{eff}}}{t_{H \rightarrow 0^+}^{\text{eff}}}\right] = N_s \Delta F = -b \left[ \left( \frac{\hat{S}}{2T} + \frac{a_1(T)}{\xi^{\theta/2}} \right) \xi^{D-(\theta/2)} H^2 + a_3(T) \xi^{2D-(3\theta/2)} H^4 + a_5(T) \xi^{3D-2\theta} H^6 + \mathcal{O}(H^8) \right] \quad (19)$$

where the coefficient  $b$  is a geometrical factor, and we have absorbed the  $k_B T$  term in the  $a_n(T)$  coefficients. The correction term  $a_1(T)/\xi^{\theta(\bar{x})/2}$  is small compared to  $\hat{S}/T$ , so it will be neglected in subsequent expressions. Equation 19 shows that the higher order terms have the functional form, in Eq. 20,

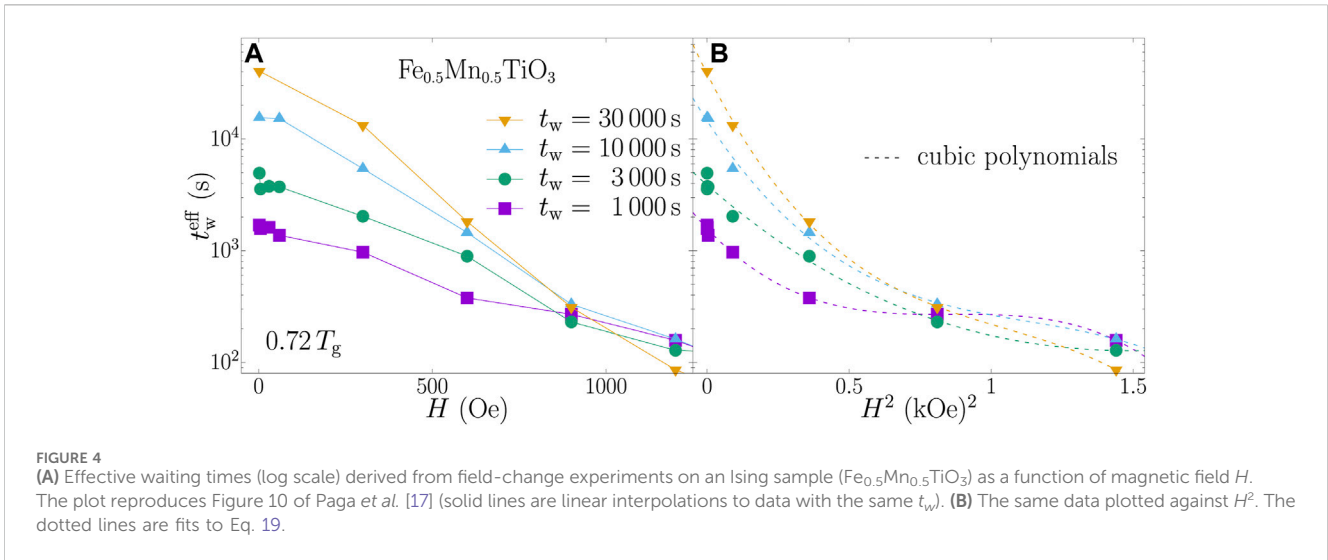
$$\chi_{2n-1} \frac{H^{2n}}{(2n)!} = a_{2n-1}(T) \xi^{-\theta(\bar{x})/2} \left[ \xi^{2\gamma_H} H^2 \right]^n \quad (20)$$

where, in Eq. 21

$$2\gamma_H = D - \frac{\theta(\bar{x})}{2} \quad (21)$$

This leads to the new scaling relation,

$$\ln\left(\frac{t_H^{\text{eff}}}{t_{H \rightarrow 0^+}^{\text{eff}}}\right) = \frac{\hat{S}}{T} \xi^{D-(\theta/2)} H^2 + \xi^{-\theta/2} \mathcal{G}\left(\xi^{D-(\theta/2)} H^2; T\right). \quad (22)$$



where the geometrical factor  $b$  has been absorbed into the scaling function  $\mathcal{G}$ ).

Among the many uses of Eq. 22, two can be highlighted. The first is the issue surrounding the magnetization encompassed in  $\xi_{\text{Zeeman}}(t_w, T)$ . The original introduction proposal, Ref. [1], envisaged the reduction of the barrier heights  $\Delta(t_w, T)$  by  $E_Z$  [Eq. 1] to be caused by the magnetization induced by the magnetic field within the volume subtended by the spin glass coherence length  $\xi(t_w, T)$ , viz Eq. 1. A subsequent treatment [33] associated  $E_Z$  with the magnetization associated with the fluctuations of the entire system of  $N$  spins, namely,  $\propto \sqrt{N}$ . The magnetic field dependence is very different, the former  $E_z \propto H^2$  while the latter  $E_Z \propto H$ .

A comparison of the two was exhibited in Fig. 10 of Ref. [17], reproduced here as Figure 4. The magnitude of the magnetic fields contained in Figure 4 are quite large. The authors of Ref. [33] state that the proportionality to  $H$  fails at low magnetic fields. The reader can judge whether a linear fit to  $H$  is obeyed by the left-hand of Figure 4. The right-hand of Figure 4 is the fit to the scaling law, valid over the full range of  $H$ , large and small. Again, the reader can judge which fit is preferable.

The second is the value of the condensation temperature,  $T_g$ . In principle, determination of  $T_g$  would require an infinite  $t_w$  because  $\xi(T) \rightarrow \infty$  when  $T \rightarrow T_g$ . One expects that any experiment at finite  $t_w$  would yield a maximum for the non-linear susceptibility at a temperature we shall call  $T_g(t_w)$  because  $t_w$  is finite.

In principle then, by measuring  $T_g(t_w)$  for ever larger  $t_w$ , one could extrapolate to the true  $t_w \rightarrow \infty$  condensation temperature  $T_g$ . If nothing else, measurements at large values of  $t_w$  on laboratory time scales could establish an upper bound for  $T_g$ .

The non-linear susceptibility  $\chi_3$  diverges as Eq. 23

$$\chi_3(t_w \rightarrow \infty; T) = \chi_0 \frac{T_g(t_w \rightarrow \infty)}{|T_g(t_w \rightarrow \infty) - T|^\gamma} \quad (23)$$

where  $\chi_0$  is a constant independent of temperature, and  $\gamma = 6.13$  (11) from Ref. [32]. For finite  $t_w$ ,  $\chi_3(t_w, T)$  only has a maximum as a function of temperature. A way of arriving at this maximum would be to fit the data to the function, in Eq. 24

$$\chi_3(t_w, T) = \chi_0 \frac{T_g(t_w)}{|T_g(t_w) - T|^\gamma} \quad (24)$$

and then use data points from just two or three temperatures to extract  $T_g(t_w)$ . For larger and larger  $t_w$ , one could in principle extrapolate to the true  $T_g$ . This is just a suggestion for a feasible process for taking laboratory data for finite  $t_w$  and extrapolating to find  $T_g(t_w \rightarrow \infty)$ .

### 2.3 Temperature chaos

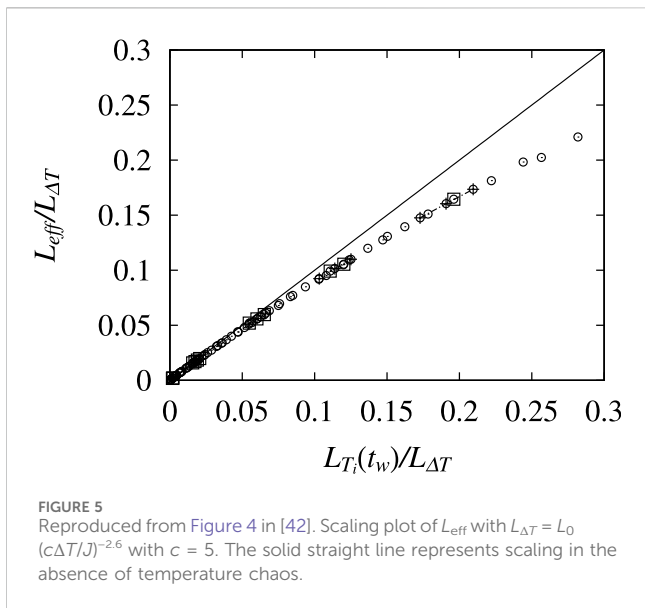
Temperature chaos is one of the outstanding mysteries posed by spin glasses. It consists of the complete reorganization of the equilibrium configurations by the slightest change in temperature.” [34] These are the opening lines of a major paper titled “Temperature chaos is a non-local effect” and set the stage for this section. Even the existence of temperature chaos in spin glasses has been questioned [35–38]. Recent experiments [39] and simulations [40] have shed light on its existence and nature, but there are many questions that remain.

From this article’s perspective, the opening gambit was the renormalization group perspective of Bray and Moore [41]. They introduced a length scale associated with temperature chaos that, for all practical purposes, can be simplified to,

$$\ell_c(T_1, T_2) = a_0 \left[ \frac{T_2}{T_1 - T_2} \right]^{1/\zeta} \quad (25)$$

where  $\zeta = d_s - \theta$ ,  $d_s$  the fractal dimension of the correlated region, and  $\theta$  is the replicon exponent. The system is in an equilibrium state at a temperature  $T_1$ , after which the temperature is dropped to  $T_2$ . Temperature chaos obtains with a length scale  $\ell_c$ . The reason that  $\ell_c$  is important is that, for a coherence length  $\xi(t_w, T)$  not infinite, temperature chaos requires a finite temperature drop. The condition is, shown in Eq. 26

$$\begin{aligned} \text{Temperature chaos: } & \ell_c(T_1, T_2) \leq \xi(t_w, T_1), \\ \text{Reversible: } & \ell_c(T_1, T_2) \geq \xi(t_w, T_1), \end{aligned} \quad (26)$$



where by “reversible” we mean that the system “remembers where it came from” when the temperature is dropped from  $T_1$  to  $T_2$ , i.e., no temperature chaos.

Though the relationship Eq. 25 is for a spin glass in equilibrium, realistically, this is never the case. Fortunately, recently an analysis was provided [40] which is titled “Temperature chaos is present in off-equilibrium spin-glass dynamics,” so that we can use the relationship Eq. 25 experimentally. Note that both  $t_w$  and  $\Delta T = T_1 - T_2$  are controllable parameters. Hence, we can probe the onset of temperature chaos by examining spin glass dynamics under difference conditions, and in particular, can control its onset.

Experiments have probed temperature chaos. The first definitive paper [42] defined the length scale for chaos as  $L_{\Delta T}$  given by Eq. 27,

$$L_{\Delta T} \sim L_0 |\Delta T / J|^{-1/\zeta} \tag{27}$$

equivalent to our Eq. 25 with  $L_{\Delta T} \equiv \ell_c(T_1, T_2)$ , and  $J$  an exchange energy in units of temperature. They extract an effective chaos length scale,  $L_{\text{eff}}$  from the following plot (their Figure 4, our Figure 5): Their plot generates  $1/\zeta = 2.6$  or  $\zeta = 0.38$ . This value is a factor of nearly 3 below the rather universally accepted value of  $\zeta = 1.1$  (see Appendix B in Ref. [39], for a full listing of theoretical values for  $\zeta$ ).

It is difficult to understand why their value for  $\zeta$  was so far off from what is now regarded as the fairly accepted value near unity. An origin may be lie in their measurement protocol, namely, a zero-field magnetization measurement where the magnetic field is applied after cycling to  $T_1$ . Magnetic field chaos [43, 44] could then be compounded with temperature chaos, and distort the extraction of a value for  $1/\zeta$ .

In order to circumvent this possibility, Zhai et al. [39] worked with a protocol where the magnetic field remained constant across temperature cycling. The idea was to use the field-cooled magnetization to investigate temperature chaos in spin glasses. This protocol involved turning on a magnetic field  $H$  above the condensation temperature,  $T_g$ , keeping it constant throughout the temperature cycling protocol.

The specific steps were as follows. The decay of the field cooled (FC) magnetization,  $M_{FC}(t, T_1, H)$  is measured at the first temperature stop  $T_1$  after cooling in the current magnetic field and waiting a time  $t_{w1}$ . The decay curve is denoted as the “reference curve.” Then, temperature cycling is engaged, where one first cools to temperature  $T_1$ , waits a time  $t_{w1}$ , cools to  $T_2$ , waits a time  $t_{w2}$ , then rapidly warms back to  $T_1$ , and measures the decay of the magnetization  $M_{FC}(t, T_1, H)$ .

In order to observe TC,  $T_1$  was fixed and the temperature  $T_2$  was gradually lowered in separate experimental runs to  $T_2 = T_1 - \Delta T$ . Following the temperature drop, if,

$$x = \frac{\ell_c(T_1, T_2)}{\xi(T_1, t_{w1})} \geq 1, \tag{28}$$

the coherence length will continue to grow, and one remains in the reversible state. However, in Eq. 29

$$x = \frac{\ell_c(T_1, T_2)}{\xi(T_1, t_{w1})} \leq 1 \tag{29}$$

temperature chaos sets in and one finds a diminished coherence length after heating back to temperature  $T_1$  (see the discussion below of memory).

As a consequence, under reversible dynamics, Eq. 28, the decay curve of  $M_{FC}(t, T_1, H)$  after temperature cycling can be superposed on the reference decay curve, allowing for a positive shift in time for  $M_{FC}(t, T_1, H)$  during the time that  $T < T_1$ . However, after the onset of temperature chaos, The decay curves cannot be superposed for any positive shift of  $M_{FC}(t, T_1, H)$  in time.

This is seen explicitly in Figure 6 which was reproduced from Figure 1 of Ref [39]. By changing  $T_1, t_{w1}$ , Eq. 25 can be probed to yield a value for  $1/\zeta$ . A value for  $\zeta \approx 1.1$  was extracted in [39], very close to a majority of the theoretical values.

This experimental evidence for the existence of temperature chaos in spin glasses will prove important in our subsequent treatments of rejuvenation and memory. We shall argue that temperature chaos is responsible for the former, and plays an important role in a quantitative treatment of the latter. In any case, the experiments of Ref. [34] have shown that temperature chaos is present in spin glasses, and will be shown to have a profound impact in other dynamical spin glass phenomena.

## 2.4 Rejuvenation

The singular publication that engendered the attention of both theorists and experimentalists for over three decades was that of Jonason et al. [45] titled “Memory and Chaos Effects in Spin Glasses.” They displayed the remarkable figure (Figure 7 reproduced from Figure 1 in their paper). The system is “aged” at 12 K, becoming “older.” Upon lowering the temperature, it returns to the reference curve, thus becoming “younger.” This is termed “rejuvenation.” It was attributed to temperature chaos, namely, the spin glass “forgot” its previous history of aging when the temperature was lowered beyond the threshold for temperature chaos.

This assignment has yet to be proven unequivocally. A very recent paper [18] by Paga et al. displayed the results of temperature cycling to explore this claim, and indeed to relate rejuvenation to the

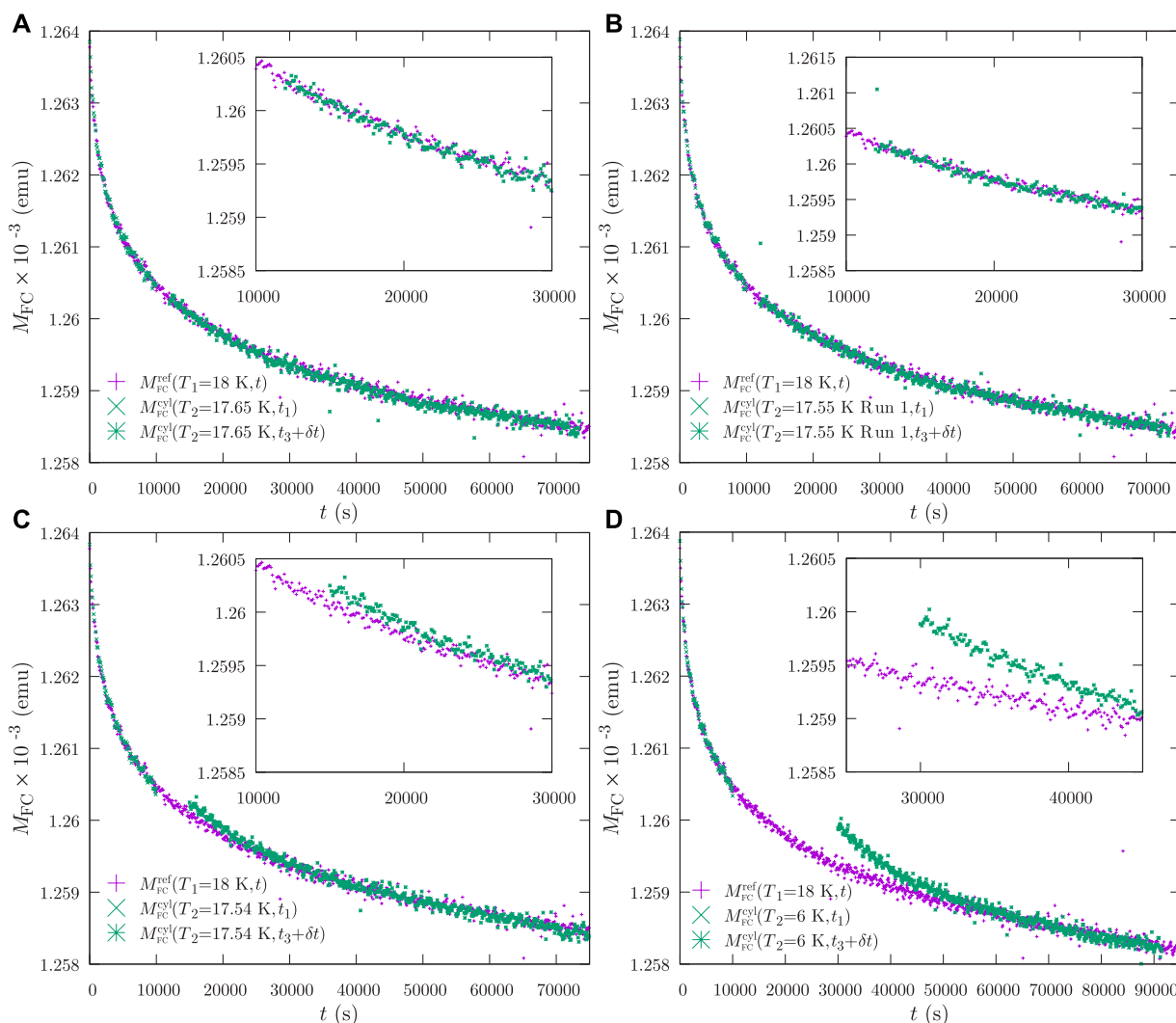


**FIGURE 6**  
 The example of  $T_1 = 18$  K, reproduced from Figure 1 in [39]. The temperature is gradually lowered to  $T_2$  after  $t_{w1} = 10^4$  s and heated back to  $T_1$  after  $t_{w2} = 10^3$  s. The temperature cycling curve is then shifted by  $\delta t$  to overlap the reference curve. In the reversible temperature range, (A) and (B) the cycling curve can be overlapped with the reference curve over the whole period  $\approx 7 \times 10^4$  s. In the chaotic range, (C) and (D), the cycling curve can only be partially overlapped. Hence, temperature chaos, at  $T_1 = 18$  K,  $t_{w1} = 10^4$  s, sets in for  $\Delta T > 450$  mK.

spin glass coherence length. Figure 8 reproduces their Figure 2. While Figure 8 appears definitive, there needs to be an exploration of  $t_w^{eff}$  for temperature above and below the temperature for the onset of temperature chaos to arrive at an unequivocal relationship between rejuvenation and temperature chaos. For the moment, Figure 8 seems entirely consistent with that interpretation.

### 2.5 Memory

Though rejuvenation in spin glasses is remarkable, the even more remarkable is memory. Once the system has rejuvenated back to the reference curve, upon reheating it traces out the same behavior as it exhibited upon cooling, even with temperature chaos between  $T_1$  and  $T_2$ . This is explicitly demonstrated in Figure 7. On the surface it seems quite inconsistent. How can the system exhibit memory when it has experienced temperature

chaos? There have been a multitude of papers and models that addressed this conundrum. Most involve heuristic models with adjustable parameters that can fit the data represented in Figure 7. A recent treatment [18] gives an interpretation that is free of real space models and the concomitant adjustable parameters, and is based upon the behavior of the spin glass coherence length. The beauty of this formulation is that every term in its interpretation can be tested experimentally, something that previous models lack.

The concept is as follows. Upon cooling the spin glass from above  $T_g$  to the first measuring temperature  $T_1$ , the system is aged for a time  $t_{w1}$ . As a consequence, the spin glass coherence length grow from nucleation to  $\xi(t_{w1}, T)$ . When the temperature is then lowered to  $T_2$ , the correlations created at  $T_1$  are essentially frozen. This concept has been introduced by Bouchaud et al. [45]. What is new is that, when the system is aged at  $T_2$  for a time  $t_{w2}$ , the system has created new coherent regions that have nothing to do with those

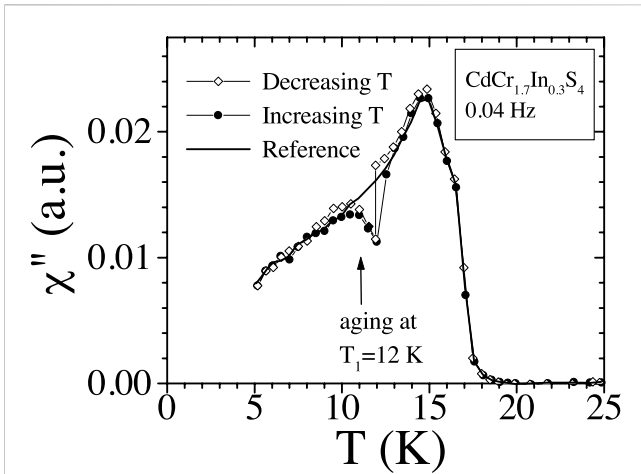


**FIGURE 7**  
 Reproduced from Figure 1 of Ref. [45]. Out-of-phase susceptibility  $\chi''$  of the  $\text{CdCr}_{1.7}\text{In}_{0.3}\text{S}_4$  spin glass. The solid line is measured upon heating the sample at a constant rate on 0.1 K/min (reference curve). Open diamonds: the measurement is done during cooling at this same rate, except that the cooling procedure has been stopped at 12 K during 7 h to allow for aging. Cooling then resumes down to 5 K;  $\chi''$  is not influenced and goes back to the reference curve (chaos). This is termed rejuvenation. Solid circles: after this cooling procedure, the data is taken while reheating at the previous constant rate, exhibiting memory of the aging stage at 12 K.

created at  $T_1$ . Hence, when heating back to  $T_2$ , the two correlated regions *interfere*, thereby reducing the spin glass coherence length from the native value created at  $T_1, t_{w1}$ .

This is exhibited explicitly in Figure 8 in the lower part of the figure. The  $C_n$  represent three separate temperature and waiting time cycles, and illustrate unequivocally the relationship between memory and competing coherence lengths. Each of the cycles has three steps: 1) the system is “prepared” at  $T_1 = 30$  K by waiting for the same time  $t_{w1} = 1$  h 2) The temperature is then dropped to  $T_2$  and the system is aged for  $t_{w2}$ . 3) The system is then heated back to  $T_1 = 30$  K and  $t_w^{\text{eff}}$  measured as rapidly as possible.  $C_1$  sets  $T_2 = 26$  K and  $t_{w2} = 1/6$  h.  $C_2$  sets  $T_2 = 26$  K and  $t_{w2} = 3$  h. Finally,  $C_3$  sets  $T_2 = 16$  K and  $t_{w2} = 3$  h. Memory is quantified by comparing the magnitude of the coherence length measured at step (3) with the native coherence length [the coherence length of the initially prepared state at step (1)]. If the two lengths are the same, memory is perfect. If after step (3), the measured coherence length is smaller than the initially prepared state at step (1), memory is less, a direct result of the interference of the two states. The slopes in Figure 8 are steeper, the larger the coherence length being measured because the volume of the correlated region is larger [Eq. 1].

Consider  $C_1$ . The system has “morphed” from the prepared state into a chaotic regime, but only aged for a short time (1/6 h). The coherence length in the chaotic state has grown during this time, so that its interference with the initially prepared coherence length is significant. Hence, the memory is less, exhibited by the shallower slope as compared to the native slope exhibited in Figure 8. Now,  $C_2$  increases  $t_{w2}$  to 3 h, so that the coherence length in the chaotic state can grow beyond its value in  $C_1$ . This should lead to greater interference, a smaller memory, and a more shallow slope than found for  $C_1$ . This is explicit in Figure 8.

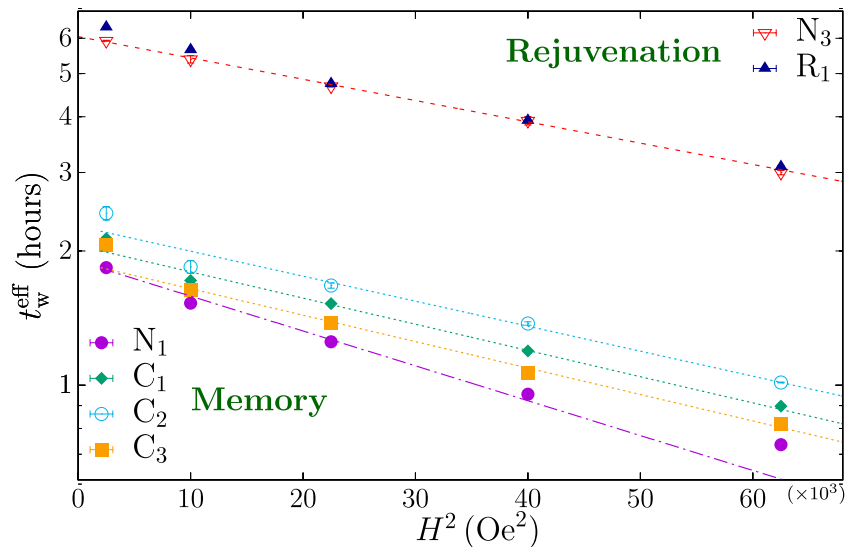


**FIGURE 8**  
 Reproduced from Figure 2 of Ref. [18]. We use the abbreviations N (native), R (rejuvenation), and C (cycle). By native, we mean the temperature is lowered from above  $T_g$  (here,  $T_g = 41.6$  K to the lower temperature  $T_2$  in the usual cycling protocol (here,  $T_2 = 26$  K,  $t_{w2} = 3$  h), and the effective waiting time is given by the peak in  $S(t)$  for different magnetic fields  $H$ . The points are labeled  $N_3$  in Figure 8. Next, the system is cooled from above  $T_g$  to the temperature  $T_1 = 30$  K and aged for 1 h. The temperature is then dropped to  $T_2 = 26$  K, and aged for 3 h. The points are labelled  $R_1$  in Figure 8. As can be seen from the figure, the two procedures yield nearly exactly the same  $t_w^{\text{eff}}$  for all values of  $H^2$ , independent of the aging at  $T_1$ . This is a clear demonstration of rejuvenation. In addition, the spin glass coherence lengths can be extracted from the slope of  $t_w^{\text{eff}}$  vs  $H^2$ . One finds  $\xi_{N_3}/a_0 = 11.96(9)$  and  $\xi_{R_1}/a_0 = 11.787(8)$ , showing the development of spin glass order is the same without and with aging at  $T_1$ . Memory is measured through a full temperature cycle, from  $T_1, t_{w1} \rightarrow T_2, t_{w2} \rightarrow T_1$  when  $t_w^{\text{eff}}$  is measured as rapidly as possible. The text discusses the physical meaning for the three protocols,  $C_1, C_2$ , and  $C_3$ .



Finally, the  $C_3$  protocol has the same  $t_{w2}$  as  $C_2$ , but the temperature drop to  $T_2$  is much greater,  $T_2 = 16$  K. At such a low temperature, the growth of the chaotic coherence length is very slow (almost none), so there should be almost no interference, and the memory should be nearly perfect. This again is explicitly exhibited in Figure 8 where the slope of  $C_3$  is close to the slope for the native slope.

These three temperature cycles, and their properties exhibited in Figure 8, are strong evidence for the interpretation of memory through interfering coherence volumes. This is at odds with Ref. [46] where it is argued that the coherence length returned to the native value upon reheating. By adjusting  $t_{w2}$  one can change the value of  $\xi(T_1, t_{w1}, T_2, t_{w2})$  at will, from no loss to complete loss of memory. This has been born out in our Figure 8, and also in independent experiments by Freedberg et al. [47].

### 3 Summary

The purpose of this paper is to display spin glass dynamics through the lens of the spin glass coherence length. We have shown how it use can unite the seeming independent features observed both in the laboratory and through simulations. They provide a unifying picture for what seem to be independent complex phenomena.

### Data availability statement

The raw data supporting the conclusions of this article will be made available by the authors, without undue reservation.

### Author contributions

JH: Visualization, Writing–original draft, Writing–review and editing. RO: Conceptualization, Data curation, Formal Analysis,

Funding acquisition, Investigation, Project administration, Resources, Supervision, Validation, Visualization, Writing–original draft, Writing–review and editing.

### Funding

The author(s) declare that financial support was received for the research, authorship, and/or publication of this article. This work has been supported by the U.S. Department of Energy, Office of Basic Energy Sciences, Division of Materials Science and Engineering, under Award DE-SC0013599.

### Acknowledgments

We thank Dr. I. Paga for a close reading of this manuscript, and for her important insights.

### Conflict of interest

The authors declare that the research was conducted in the absence of any commercial or financial relationships that could be construed as a potential conflict of interest.

The handling editor FRT declared a past co-authorship with the author RO.

### Publisher's note

All claims expressed in this article are solely those of the authors and do not necessarily represent those of their affiliated organizations, or those of the publisher, the editors and the reviewers. Any product that may be evaluated in this article, or claim that may be made by its manufacturer, is not guaranteed or endorsed by the publisher.

### References

- Joh YG, Orbach R, Wood GG, Hammann J, Vincent E. Extraction of the spin glass correlation length. *Phys Rev Lett* (1999) 82:438–41. doi:10.1103/PhysRevLett.82.438
- Marinari E, Parisi G, Ruiz-Lorenzo J, Ritort F. Numerical evidence for spontaneously broken replica symmetry in 3d spin glasses. *Phys Rev Lett* (1996) 76:843–6. doi:10.1103/PhysRevLett.76.843
- Baity-Jesi M, Calore E, Cruz A, Fernandez LA, Gil-Narvion JM, Gordillo-Guerrero A, et al. Matching microscopic and macroscopic responses in glasses. *Phys Rev Lett* (2017) 118:157202. doi:10.1103/PhysRevLett.118.157202
- Sherrington D, Kirkpatrick S. Solvable model of a spin-glass. *Phys Rev Lett* (1975) 35:1792–6. doi:10.1103/PhysRevLett.35.1792
- Mézard M, Parisi G, Sourlas N, Toulouse G, Virasoro M. Replica symmetry breaking and the nature of the spin glass phase. *J Phys France* (1984) 45:843–54. doi:10.1051/jphys:01984004505084300
- Parisi G. Spin glasses and fragile glasses: statics, dynamics, and complexity. *Proc Natl Acad Sci* (2006) 103:7948–55. doi:10.1073/pnas.0601120103
- Parisi G. Toward a mean field theory for spin glasses. *Phys Lett A* (1979) 73:203–5. doi:10.1016/0375-9601(79)90708-4
- Parisi G. A sequence of approximated solutions to the s-k model for spin glasses. *J Phys A: Math Gen* (1980) 13:L115–21. doi:10.1088/0305-4470/13/4/009
- Hammann J, Lederman M, Ocio M, Orbach R, Vincent E. Spin-glass dynamics Relation between theory and experiment: a beginning. *Physica A Stat Mech its Appl* (1992) 185:278–94. doi:10.1016/0378-4371(92)90467-5
- Nordblad P, Svedlindh P, Lundgren L, Sandlund L. Time decay of the remanent magnetization in a cumn spin glass. *Phys Rev B* (1986) 33:645–8. doi:10.1103/PhysRevB.33.645
- Baity-Jesi M, Baños R, Cruz A, Fernandez L, Gil-Narvion J, Gordillo-Guerrero A, et al. Janus ii: a new generation application-driven computer for spin-system simulations. *Comput Phys Commun* (2014) 185:550–9. doi:10.1016/j.cpc.2013.10.019
- Baity-Jesi M, Calore E, Cruz A, Fernandez LA, Gil-Narvion JM, Gonzalez-Adalid Pemartin I, et al. Memory and rejuvenation effects in spin glasses are governed by more than one length scale. *Nat Phys* (2023) 19:978–85. doi:10.1038/s41567-023-02014-6
- de Almeida JRL, Thouless DJ. Stability of the sherrington-kirkpatrick solution of a spin glass model. *J Phys A: Math Gen* (1978) 11:983–90. doi:10.1088/0305-4470/11/5/028
- De Dominicis C, Giardinà I. *Random fields and spin glasses: a field theory approach*. Cambridge University Press (2006). doi:10.1017/CBO9780511534836
- Belletti F, Cotallo M, Cruz A, Fernandez LA, Gordillo-Guerrero A, Guidetti M, et al. Nonequilibrium spin-glass dynamics from picoseconds to a tenth of a second. *Phys Rev Lett* (2008) 101:157201. doi:10.1103/PhysRevLett.101.157201
- Belletti F, Cruz A, Fernandez LA, Gordillo-Guerrero A, Guidetti M, Maiorano A, et al. An in-depth view of the microscopic dynamics of ising spin glasses at fixed temperature. *J Stat Phys* (2009) 135:1121–58. doi:10.1007/s10955-009-9727-z
- Paga I, Zhai Q, Baity-Jesi M, Calore E, Cruz A, Fernandez LA, et al. Spin-glass dynamics in the presence of a magnetic field: exploration of microscopic properties. *J Stat Mech Theor Exp* (2021) 2021:033301. doi:10.1088/1742-5468/abdafa

18. Collaboration J, Paga I, He J, Baity-Jesi M, Calore E, Cruz A, et al. *arxiv: quantifying memory in spin glasses* (2023).
19. Paga I, Zhai Q, Baity-Jesi M, Calore E, Cruz A, Cummings C, et al. Superposition principle and nonlinear response in spin glasses. *Phys Rev B* (2023) 107:214436. doi:10.1103/PhysRevB.107.214436
20. Koper GJM, Hilhorst HJ. A domain theory for linear and nonlinear aging effects in spin glasses. *J Phys France* (1988) 49:429–43. doi:10.1051/jphys:01988004903042900
21. Fisher DS, Huse DA. Nonequilibrium dynamics of spin glasses. *Phys Rev B* (1988) 38:373–85. doi:10.1103/PhysRevB.38.373
22. Baity-Jesi M, Calore E, Cruz A, Fernandez LA, Gil-Narvion JM, Gordillo-Guerrero A, et al. Aging rate of spin glasses from simulations matches experiments. *Phys Rev Lett* (2018) 120:267203. doi:10.1103/PhysRevLett.120.267203
23. Zinn-Justin J. Quantum field theory and critical phenomena. In: *International series of monographs on physics*. Oxford University Press (2021). General theoretical arguments suggest that  $z_c$  is also  $\xi$  independent at exactly  $T = T_g$ .
24. Zhai Q, Harrison DC, Tennant D, Dahlberg ED, Kenning GG, Orbach RL. Glassy dynamics in cumm thin-film multilayers. *Phys Rev B* (2017) 95:054304. doi:10.1103/PhysRevB.95.054304
25. Kenning GG, Tennant DM, Rost CM, da Silva FG, Walters BJ, Zhai Q, et al. End of aging as a probe of finite-size effects near the spin-glass transition temperature. *Phys Rev B* (2018) 98:104436. doi:10.1103/PhysRevB.98.104436
26. Zhai Q, Martin-Mayor V, Schlagel DL, Kenning GG, Orbach RL. Slowing down of spin glass correlation length growth: simulations meet experiments. *Phys Rev B* (2019) 100:094202. doi:10.1103/PhysRevB.100.094202
27. Malozemoff AP, Barbara B, Imry Y. Further studies of nonlinear susceptibility of GdAl and MnCu spin glasses. *J Appl Phys* (1982) 53:2205–7. doi:10.1063/1.330818
28. Malozemoff AP, Imry Y, Barbara B. Scaling of susceptibility and the size of the critical region in an amorphous GdAl spin glass (invited). *J Appl Phys* (1982) 53:7672–7. doi:10.1063/1.330179
29. Chandra P, Coleman P, Ritchey I. The anisotropic kagome antiferromagnet: a topological spin glass? *J Phys France* (1993) 3:591–610. doi:10.1051/jp1:1993104
30. Lévy LP, Ogielski AT. Nonlinear dynamic susceptibilities at the spin-glass transition of ag:mn. *Phys Rev Lett* (1986) 57:3288–91. doi:10.1103/PhysRevLett.57.3288
31. Lévy LP. Critical dynamics of metallic spin glasses. *Phys Rev B* (1988) 38:4963–73. doi:10.1103/PhysRevB.38.4963
32. Baity-Jesi M, Baños RA, Cruz A, Fernandez LA, Gil-Narvion JM, Gordillo-Guerrero A, et al. Critical parameters of the three-dimensional ising spin glass. *Phys Rev B* (2013) 88:224416. doi:10.1103/PhysRevB.88.224416
33. Bert F, Dupuis V, Vincent E, Hammann J, Bouchaud JP. Spin anisotropy and slow dynamics in spin glasses. *Phys Rev Lett* (2004) 92:167203. doi:10.1103/PhysRevLett.92.167203
34. Fernandez LA, Marinari E, Martin-Mayor V, Parisi G, Yllanes D. Temperature chaos is a non-local effect. *J Stat Mech Theor Exp* (2016) 2016:123301. doi:10.1088/1742-5468/2016/12/123301
35. Sasaki M, Nemoto K. Memory effect, rejuvenation and chaos effect in the multi-layer random energy model. *J Phys Soc Jpn* (2000) 69:2283–90. doi:10.1143/JPSJ.69.2283
36. Sasaki M, Martin OC. Discreteness and entropic fluctuations in generalized-random-energy-model-like systems. *Phys Rev B* (2002) 66:174411. doi:10.1103/PhysRevB.66.174411
37. Sales M, Bouchaud JP, Ritort F. Temperature shifts in the sinai model: static and dynamical effects. *J Phys A: Math Gen* (2003) 36:665–84. doi:10.1088/0305-4470/36/3/306
38. Rizzo T. Ultrametricity between states at different temperatures in spin-glasses. *Eur Phys J B* (2002) 29:425–35. doi:10.1140/epjb/e2002-00274-x
39. Zhai Q, Orbach RL, Schlagel DL. Evidence for temperature chaos in spin glasses. *Phys Rev B* (2022) 105:014434. doi:10.1103/PhysRevB.105.014434
40. Baity-Jesi M, Calore E, Cruz A, Fernandez LA, Gil-Narvion J, Gonzalez-Adalid Pemartin I, et al. Temperature chaos is present in off-equilibrium spin-glass dynamics. *Commun Phys* (2021) 4:74. doi:10.1038/s42005-021-00565-9
41. Bray AJ, Moore MA. Chaotic nature of the spin-glass phase. *Phys Rev Lett* (1987) 58:57–60. doi:10.1103/PhysRevLett.58.57
42. Jönsson PE, Yoshino H, Nordblad P. Symmetrical temperature-chaos effect with positive and negative temperature shifts in a spin glass. *Phys Rev Lett* (2002) 89:097201. doi:10.1103/PhysRevLett.89.097201
43. Kondor I. On chaos in spin glasses. *J Phys A: Math Gen* (1989) 22:L163–8. doi:10.1088/0305-4470/22/5/005
44. Billoire A, Coluzzi B. Magnetic field chaos in the sherrington-kirkpatrick model. *Phys Rev E* (2003) 67:036108. doi:10.1103/PhysRevE.67.036108
45. Jonason K, Vincent E, Hammann J, Bouchaud JP, Nordblad P. Memory and chaos effects in spin glasses. *Phys Rev Lett* (1998) 81:3243–6. doi:10.1103/PhysRevLett.81.3243
46. Bouchaud JP, Dupuis V, Hammann J, Vincent E. Separation of time and length scales in spin glasses: temperature as a microscope. *Phys Rev B* (2001) 65:024439. doi:10.1103/PhysRevB.65.024439
47. Freedberg J, Meese WJ, He J, Schlagel DL, Dahlberg ED, Orbach RL. *arxiv: on the nature of memory and rejuvenation in glassy systems* (2023).